

Passivation of silicon surfaces by heat treatment in liquid water at 110 °C

Tomohiko Nakamura¹, Toshiyuki Sameshima¹, Masahiko Hasumi¹, and Tomohisa Mizuno²

¹Tokyo University of Agriculture and Technology, Koganei, Tokyo 184-8588, Japan

²Kanagawa University, Hiratsuka, Kanagawa 259-1293, Japan

E-mail: tsamesim@cc.tuat.ac.jp

Received December 20, 2014; accepted July 24, 2015; published online September 16, 2015

We report the effective passivation of silicon surfaces by heating single-crystalline silicon substrates in liquid water at 110 °C for 1 h. High photo-induced effective minority carrier lifetimes τ_{eff} were obtained ranging from 8.3×10^{-4} to 3.1×10^{-3} s and from 1.2×10^{-4} to 6.0×10^{-4} s for the n- and p-type samples, respectively, under 635 nm light illumination, while the τ_{eff} values of the initial bare samples were lower than 1.2×10^{-5} s. The heat treatment in liquid water at 110 °C for 1 h resulted in low surface recombination velocities ranging from 7 to 34 cm/s and from 49 to 250 cm/s for the n- and p-type samples, respectively. The photo-conductivity of the n-type sample was increased from 3.8×10^{-3} (initial) to 1.4×10^{-1} S/cm by the present heat treatment under air-mass (AM) 1.5 light illumination at 100 mW/cm². The thickness of the passivation layer was estimated to be only approximately 0.7 nm. Metal-insulator-semiconductor-type solar cells were demonstrated with Al and Au metal formation on the passivated surface. Rectified current voltage and solar cell characteristics were observed. The open circuit voltages were obtained to be 0.52 and 0.49 V under AM 1.5 light illumination at 100 mW/cm² for the n- and p-type samples, respectively.

© 2015 The Japan Society of Applied Physics

1. Introduction

The passivation of silicon surfaces is important to achieve a long lifetime of photo-induced minority carriers, which is required for fabricating high-performance photo-sensors and photovoltaic devices.^{1–19)} Many technologies of surface passivation have been developed. The formation of thermally grown SiO₂ layers above 1000 °C gives a very stable SiO₂/Si interface with a low density of carrier recombination defects.²⁰⁾ Hydrogenation treatment is a useful passivation method at low temperatures.^{21,22)} Hydrogen atoms terminate dangling bonds at silicon surfaces and decrease surface recombination velocity. However, passivation by hydrogenation is unstable owing to the oxidation of Si–H bonds. Silicon nitride SiN formation in plasma chemical vapor deposition has been widely used for passivation at low temperatures.²³⁾ Although the interface of SiN/Si has a high density of carrier trap states, a high density of fixed charges in SiN layer causes the field-effect-band bending of n-type silicon and accumulates electron carriers at the interface, which decreases the surface recombination velocity of n-type silicon. To achieve the passivation of p-type silicon, research on insulating materials with negative fixed charges has been actively conducted.²⁴⁾ Aluminum oxide is a practical candidate. We have reported that high-pressure H₂O vapor heat treatment is effective for decreasing surface recombination velocity at the SiO_x/Si interface at low temperatures.^{25–30)} Oxygen vacancies in SiO_x layers and interfaces have been effectively oxidized in high-pressure H₂O vapor. The formation of a thin passivation layer with a low recombination velocity and a low density of fixed charges at low temperatures is still attractive for metal-insulator-semiconductor (MIS) type devices.^{31–33)} A thin insulating layer on the order of 1 nm is required to collect electrical current from a semiconductor to a metal associated with the quantum tunneling effect.³⁴⁾ The development in low-temperature, low-cost, and simple processing is also demanded in production stages.

In this paper, we report a simple and effective passivation method performed at a low temperature of 110 °C for silicon surfaces. We demonstrate a high photo-induced minority carrier effective lifetime τ_{eff} by heating single-crystalline

Table I. Sample description.

	Resistivity (Ω cm)	Type	Surface
Sample 1	8	N	100-nm-thick thermally grown SiO ₂
Sample 2	17	N	Bare
Sample 3	15	P	Bare
Sample 4	1.7	N	Bare

silicon in liquid water at 110 °C for 1 h. The τ_{eff} achieved by the present work is compared with that of a sample coated with thermally grown SiO₂ to discuss the passivation effect of the present method. We also report high τ_{eff} values over a large area of 4-in.-sized samples. We show that the τ_{eff} maintains high values for a long time. Moreover, we demonstrate a marked increase in the photo-induced electrical conductivity of silicon samples by the present passivation. The structural analysis results show that heat treatment in liquid water at 110 °C forms an oxide passivation layer with a thickness of approximate 0.7 nm on silicon surfaces. Finally, we report the characteristics of a MIS-type solar cell fabricated using the present passivation method.

2. Experimental procedure

Four kinds of samples were prepared, as shown in Table I. Sample 1 is an 8 Ω cm n-type silicon substrate with a thickness of 500 μ m and a (100) crystalline orientation coated with 100-nm-thick thermally grown SiO₂ layers by heating in a wet atmosphere at 1100 °C. Sample 2 is a 17 Ω cm n-type silicon substrate with a thickness of 500 μ m and a (100) crystalline orientation with bare surfaces. Sample 3 is a 15 Ω cm p-type silicon substrate with a thickness of 500 μ m and a (100) crystalline orientation with bare surfaces. Sample 4 is a 1.7 Ω cm n-type silicon substrate with a thickness of 500 μ m and a (100) crystalline orientation with bare surfaces. Thermally grown SiO₂ layers and native oxide layers of the samples surfaces were initially removed by dipping the samples in 5%-diluted hydrofluoric acid. After rinsing the samples with pure and deoxidized water, they were then placed in a pressure-proof chamber with a capacity of 2800

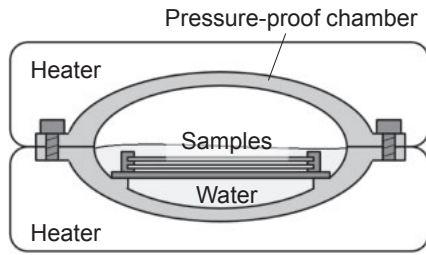


Fig. 1. Schematic of pressure-proof apparatus and image of heat treatment in liquid water at 110°C.

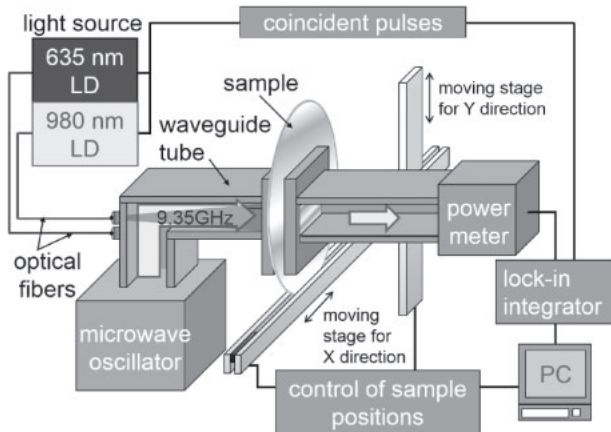


Fig. 2. Schematic of apparatus for 9.35 GHz microwave transmittance measurement system for measuring τ_{eff} of sample wafers with 635 and 980 nm light illuminations.

cm³ with 1500 cm³ of pure water. A hot-wall-type heater was used to heat the silicon samples dipped in water at 110 °C for 1 h, as shown in Fig. 1. The pressure-proof chamber kept the liquid water at 110 °C at a pressure of 2.4×10^5 Pa given by the vaporization of some of the hot water.

In order to measure τ_{eff} precisely, we used a 9.35 GHz microwave transmittance measurement system,^{35–37} as shown in Fig. 2. The system had waveguide tubes, which had a narrow gap for placing a sample for τ_{eff} measurement. Continuous-wave (CW) 635 and 980 nm laser diode (LD) lights were introduced into the waveguide tube. Microwave transmission was detected and analyzed to obtain τ_{eff} in a dark field and under LD light illumination. The penetration depth at 635 nm was about 3 μm, while it was very deep of 125 μm for 980 nm light.³⁸ The X–Y moving stage moved the sample to measure the τ_{eff} spatial distribution over the 4-in.-sized samples. The τ_{eff} of sample 1 with the SiO₂ layers coated on the surfaces was measured under 635 nm laser light illumination at 0.74 mW/cm². The SiO₂ layers were then removed by dipping the samples in 5%-diluted hydrofluoric acid and bare surfaces were formed. τ_{eff} was measured again on the seventh day, keeping the sample in air atmosphere at room temperature after the SiO₂ removal. The sample was then heated in 110 °C liquid water for 1 h. τ_{eff} was also measured three days after the 110 °C liquid water treatment. The τ_{eff} values of samples 2–4 with bare surfaces were measured under 635 and 980 nm laser light illuminations. Native oxide layers were removed by dipping the samples in 5%-diluted hydrofluoric acid. The samples were then

immediately heated in 110 °C liquid water for 1 h. τ_{eff} was also measured, and the samples were kept in air atmosphere at room temperature.

We constructed a finite element numerical calculation program including theories of carrier generation associated with optical absorption coefficients, carrier diffusion, and annihilation to estimate the surface recombination velocity S at the top and rear surfaces.^{35–39} The most possible S was determined by the best coincidence between the experimental and calculated τ_{eff} values. Because τ_{eff} is a coefficient between the carrier generation ratio per unit area G and the density of minority carriers per unit area n , as $n = \tau_{\text{eff}} \times G$, an increase in τ_{eff} causes an increase in n . An increase in n therefore causes an increase in the photo-induced carrier conductivity. We measured the photo-induced electrical conductivity to confirm the increase in photo-induced carrier density by the present treatment. Al electrodes with an area of 1×1 mm² and a gap of 1.5 mm were formed for the n-type initial and 110 °C-liquid-water-heated sample 2 by vacuum evaporation. Photo-conductivity was obtained from the electrical current under AM 1.5 light illumination at 100 mW/cm² subtracted by the electrical current in the dark field.

To analyze the thickness and structure of the passivation layers, in-depth profiles of the atomic concentrations of silicon, oxygen, and hydrogen atoms for the n-type initial and 110 °C-liquid-water-heated sample 2 were measured using high resolution Rutherford backscattering spectrometry (HR-RBS) and high resolution hydrogen forward scattering spectrometry (HR-HFS). The incidence ions and their energies were ⁴He⁺ and 450 keV for HR-RBS, and N₂⁺ and 240 keV for HR-HFS, respectively. Those measurements were carried out by Toray-Research.

Finally, we fabricated MIS-type solar cells.^{31–33} After heat treatment in liquid water at 110 °C, stripe electrodes of Al and Au with widths of 250 and 150 μm and a gap of 200 μm for sample 2, and 300 and 100 μm and a gap of 200 μm for sample 3 were formed on a top passivated surface by vacuum evaporation. The current density as a function of applied voltage was measured in a dark field and under AM 1.5 light illumination at 100 mW/cm² to the rear surface.

3. Results and discussion

Figure 3 shows the change in τ_{eff} for sample 1 coated with thermally grown SiO₂ layers, with bare surfaces obtained by removing SiO₂ layers with 5%-diluted hydrofluoric acid, and treated with 110 °C liquid water treatment. τ_{eff} was high of 2.7×10^{-3} s for the sample coated with thermally grown SiO₂ layers. This means that the silicon surfaces were well passivated by the thermally grown SiO₂ layers. We analyzed the surface recombination velocity S by fitting the calculated τ_{eff} to experimental values using a finite element numerical calculation program under the assumption of a sufficiently high bulk lifetime τ_b of 0.01 s, in which S at both surfaces determined τ_{eff} . S was estimated to be 6 cm/s. In this case of low S , τ_{eff} is given by a well-known relation with τ_b as

$$\frac{1}{\tau_{\text{eff}}} = \frac{1}{\tau_b} + \frac{2S}{d}. \quad (1)$$

The low S allows photo-induced carriers to diffuse well through the whole substrate thickness. $2S$ from the two (top and rear) surfaces determines τ_{eff} .⁴⁰

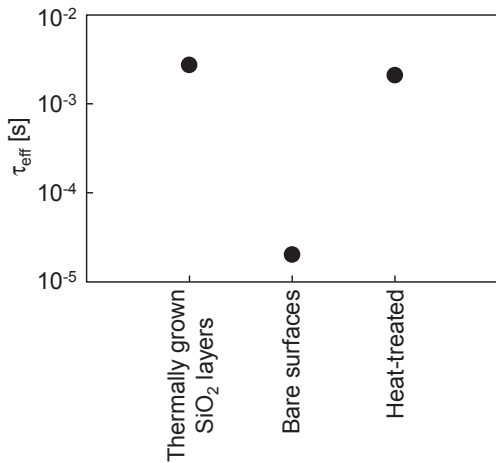


Fig. 3. Change in τ_{eff} for sample 1 coated with thermally grown SiO_2 layers, with bare surfaces obtained by removing SiO_2 layers with 5%-diluted hydrofluoric acid, and treated with 110 °C liquid water treatment under 635 nm light illumination.

On the other hand, τ_{eff} markedly decreased to 2.0×10^{-5} s for the sample with bare surfaces. A high density of carrier recombination defects was generated at the bare surfaces during keeping the sample in air atmosphere after the 5%-diluted hydrofluoric acid treatment. S was estimated to be high value of 1250 cm/s. In contrast to the low S , a high S rapidly decreases the density of photo-induced carriers in the surface region under light illumination. τ_{eff} strongly depends on carrier diffusion from the carrier generation region to the surface. Illumination with 635 nm light with a penetration depth at 2.7 μm slightly increases τ_{eff} by diffusion to the surface. Analysis method including carrier diffusion and light penetration depth therefore should be developed for the precise estimation of S .^{16–18,37} The subsequent 110 °C liquid water treatment increased τ_{eff} to 2.1×10^{-3} s, which was slightly lower than that of the initial sample coated with thermally grown SiO_2 layers. The carrier recombination defects at the bare surfaces were effectively passivated by the present 110 °C liquid water treatment. S was estimated to be 10 cm/s, which was comparable to that of the initial sample coated with thermally grown SiO_2 layers.

τ_{eff} were measured under 635 and 980 nm light illuminations over the 4-in.-sized substrates for the initial bare silicon samples 2 and 3. Low τ_{eff} values ranging from 5.9×10^{-7} to 1.2×10^{-5} s and from 2.2×10^{-5} to 3.1×10^{-5} s were obtained under 635 and 980 nm light illuminations. These results show that the initial bare sample 2 had high densities of recombination defect states in its surface region. The fact of high τ_{eff} under 980 nm light illumination results from that it takes time for photo-induced carriers generated in deep region to diffuse to the defective surface. The τ_{eff} of the initial bare sample 3 showed a similar trend. It ranged from 1.0×10^{-7} to 5.1×10^{-6} s and from 2.6×10^{-6} to 9.6×10^{-6} s under 635 and 980 nm light illuminations. The initial p-type sample also had high densities of recombination defect states in the silicon surface region. Figure 4 shows the τ_{eff} spatial distributions for the 4-in.-sized sample 2 (a) and sample 3 (b) heated in liquid water at 110 °C for 1 h under 635 nm light illumination. The edge regions with 1.2 cm did not show τ_{eff} . Accurate measurement was not possible in the

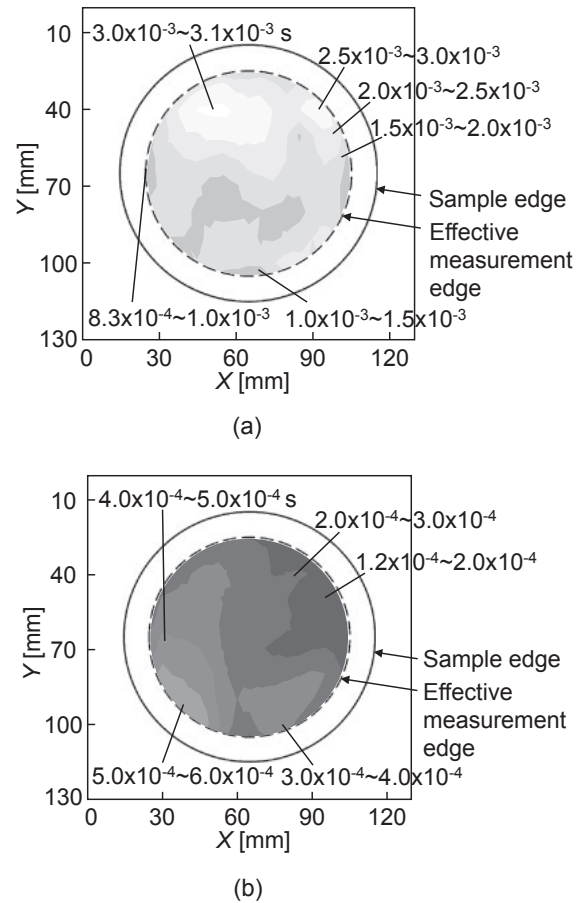


Fig. 4. τ_{eff} spatial distribution for the 4-in.-sized sample 2 (a) and sample 3 (b) heated in liquid water at 110 °C for 1 h under 635 nm light illumination. The edge regions with 1.2 cm did not show τ_{eff} because out of accurate measurement.

edge regions because of our microwave tube with a cross section of $2.3 \times 1.0 \text{ cm}^2$. τ_{eff} for sample 2 markedly increased in the range from 8.3×10^{-4} to 3.1×10^{-3} s. τ_{eff} for sample 3 also increased in the range from 1.2×10^{-4} to 6.0×10^{-4} s. The results in Fig. 4 clearly show that the silicon surfaces were well passivated by the heat treatment in liquid water at 110 °C for 1 h over a 4-in.-sized area. We also measured τ_{eff} under 980 nm light illumination. They had almost the same values as those under the 635 nm light illumination for samples 2 and 3, as shown in Fig. 4. A high τ_{eff} results in a large diffusion length of the minority carriers. When the diffusion length is much larger than the light penetration depths for the 635 and 980 nm light, the τ_{eff} values of the two different-wavelength light illuminations become coincident. S ranged from 5000 to 10000 cm/s and from 30000 to 50000 cm/s (analysis limit) for the initial samples 2 and 3. The S values were markedly decreased in the range from 7 to 34 cm/s and from 49 to 250 cm/s by the heat treatment in liquid water for samples 2 and 3, respectively. The density of recombination defect states in the sample surface regions was markedly decreased and a good passivation effect was achieved over the 4-in.-sized samples by the present heat treatment.

Figure 5 shows the τ_{eff} spatial distributions for the 4-in.-sized sample 2 (a) and sample 3 (b) at 200 h after heat treatment under 635 nm light illumination. The τ_{eff} of sample 2 maintained high values in the range from

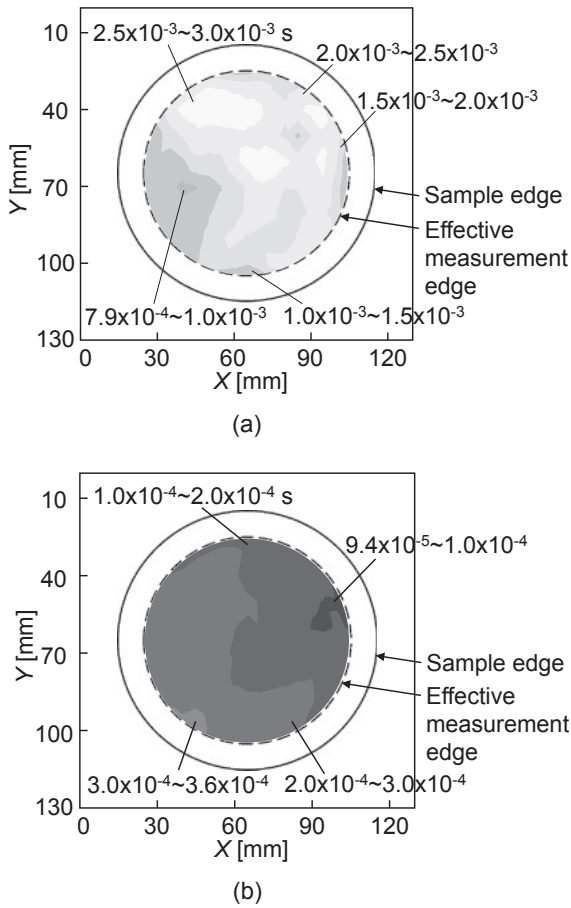


Fig. 5. τ_{eff} spatial distributions for the 4-in.-sized sample 2 (a) and sample 3 (b) at 200 h after heat treatment under 635 nm light illumination.

7.9×10^{-4} to 3.0×10^{-3} s. The τ_{eff} of sample 3 also kept high values in the range from 9.4×10^{-5} to 3.6×10^{-4} s. The S kept low values in the range from 10 to 35 cm/s and from 81 to 300 cm/s for samples 2 and 3, respectively. The τ_{eff} values under 980 nm light illumination were almost the same as those under the 635 nm light illumination for samples 2 and 3, as shown in Fig. 5. These results in Figs. 4 and 5 show that surface passivation by the present heat treatment in liquid water was maintained for a long time over a large area.

Figure 6 shows changes in the average τ_{eff} of 108 points over the 4-in. substrate with elapsed time during keeping sample 2 (a) and sample 3 (b) at room temperature in air atmosphere after heat treatment in liquid water at 110 °C for 1 h under 635 nm light illumination. The τ_{eff} values of the initial sample before the present treatment are also presented by arrows in Fig. 6. The average τ_{eff} was 1.9×10^{-3} s just after heat treatment and maintained a high value of 1.2×10^{-3} s at 570 h after heat treatment for sample 2. It was 2.9×10^{-4} s just after heat treatment and maintained 2.5×10^{-4} s at 570 h after heat treatment for sample 3. This shows that the present heat treatment in liquid water has a capability of stable passivation of silicon surfaces with low recombination defect states. It will be valuable to further search for the optimum condition of the temperature of liquid water and the duration of heat treatment to achieve a higher and more stable τ_{eff} .

Figure 7 shows the τ_{eff} for the initial and liquid-water-heated-at-110 °C-for-1-h sample 2 with 17 Ω cm and

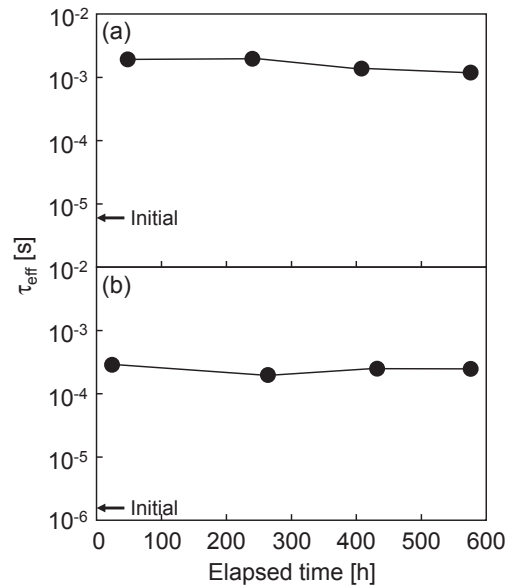


Fig. 6. The average τ_{eff} of 108 points over the 4-in. substrate with elapsed time during keeping sample 2 (a) and sample 3 (b) at room temperature in air atmosphere after heat treatment in liquid water at 110 °C for 1 h under 635 nm light illumination.

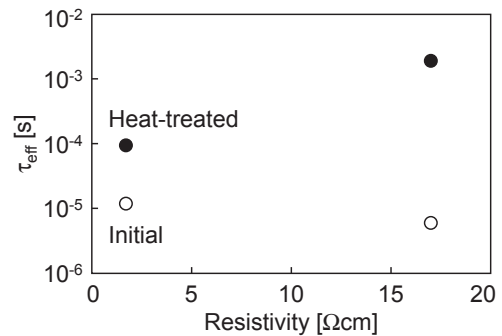


Fig. 7. τ_{eff} for the samples 2 and 4 initial and heated in liquid water at 110 °C for 1 h under 635 nm light illumination.

sample 4 with 1.7 Ω cm under 635 nm light illumination. Although the initial samples 2 and 4 had low τ_{eff} values of 6.0×10^{-6} and 1.2×10^{-5} s, their τ_{eff} values were increased to 1.9×10^{-3} and 9.5×10^{-5} s, respectively, by heat treatment in liquid water at 110 °C for 1 h. τ_{eff} under 980 nm light illumination showed almost the same trend as those under 635 nm light illumination. These results demonstrate that the present heat treatment in liquid water at 110 °C for 1 h is effective for the surface passivation of the silicon substrate with different resistivities.

We summarize the experimental values of τ_{eff} and numerically analyzed values of S for samples 1–4 in Table II. τ_{eff} were markedly increased and S were decreased by the present heat treatment compared with those of the initial samples with bare surfaces for every resistivity and carrier type. These results show that the present heat treatment was effective for the surface passivation of different kinds of single-crystalline silicon substrates.

The application of bias voltage to Al gap electrodes formed on the initial surface and the present passivated surface of sample 2 showed current–voltage characteristics with good ohmic characteristics. Figure 8 shows the photo-conductivity

Table II. Summary of τ_{eff} and S values of samples.

	Surface	τ_{eff} (s)	S (cm/s)
Sample 1	Liquid water treated	2.1×10^{-3}	10
	Bare	2.0×10^{-5}	1250
	100-nm-thick thermally grown SiO ₂	2.7×10^{-3}	6
Sample 2	Liquid water treated	8.3×10^{-4} – 3.1×10^{-3}	7–34
	Liquid water treated ^{a)}	7.9×10^{-4} – 3.0×10^{-3}	10–35
	Bare	5.9×10^{-7} – 1.2×10^{-5}	5000–10000
Sample 3	Liquid water treated	1.2×10^{-4} – 6.0×10^{-4}	49–250
	Liquid water treated ^{a)}	9.4×10^{-5} – 3.6×10^{-4}	81–300
	Bare	1.0×10^{-7} – 5.1×10^{-6}	30000–50000
Sample 4	Liquid water treated	9.5×10^{-5}	210
	Bare	1.2×10^{-5}	2900

a) Samples were kept in air atmosphere for 200h after the liquid water treatment.

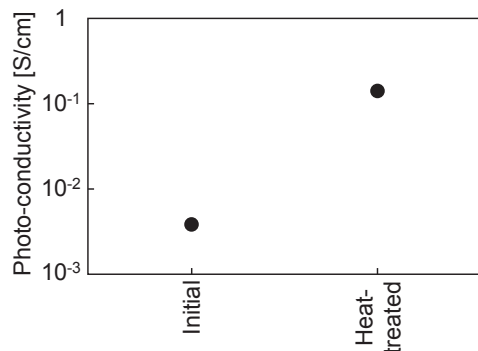


Fig. 8. Photo-conductivity at applied voltage of 2 V under AM 1.5 light illumination at 100 mW/cm² for the initial and heat treated sample 2.

at the applied voltage of 2 V for the initial and 110 °C-liquid-water-heated sample 2. The photo-conductivity was increased from 3.8×10^{-3} (initial) to 1.4×10^{-1} S/cm by the present heat treatment. Assuming that the minority carrier mobility of hole is $400 \text{ cm}^2 \text{ V}^{-1} \text{ s}^{-1}$, the carrier surface density n_{AM} was roughly estimated to be $3.0 \times 10^{12} \text{ cm}^{-2}$ for the initial sample and $1.1 \times 10^{14} \text{ cm}^{-2}$ for the heat-treated sample. Considering the high reflectivity on the sample surface, the photon flux estimated from the AM 1.5 spectra at 100 mW/cm² was about $1.8 \times 10^{17} \text{ cm}^{-2} \text{ s}^{-1}$. n_{AM} and photon flux result in τ_{eff} values of 1.7×10^{-5} s for the initial sample and 6.2×10^{-4} s for the heat-treated sample. These τ_{eff} values are rough estimates but not much different from the results of our precise analysis by microwave transmittance measurement shown in Fig. 4. The present passivation method effectively increases the photo-conductivity under the AM 1.5 light illumination by increasing photo-induced carrier density and lifetime. Moreover, a thin passivation layer allowed for current to flow via the tunneling effect at a low voltage application. This will be important for the design of MIS-type devices.⁴¹⁾

Figure 9 shows in-depth profiles of the atomic concentrations of silicon, Si (solid black curve), oxygen, O (solid gray curve), and hydrogen atoms, H (dashed curve) for sample 2 heated in liquid water at 110 °C for 1 h (a) and the initial sample (b). Very thin surface regions with a high oxygen concentration was observed for the sample

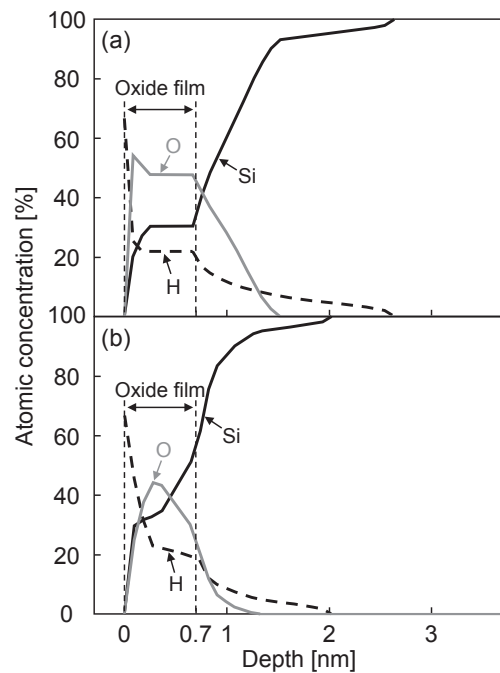


Fig. 9. In-depth profiles of the atomic concentrations of silicon (Si), oxygen (O), and hydrogen (H) atoms for sample 2 heated in liquid water at 110 °C for 1 h (a) and the initial sample (b) analyzed by HR-RBS and HR-HFS.

treated with the present passivation. Hydrogen atoms at a concentration higher than 10^{21} cm^{-3} were also distributed in the surface region. According to suggestions of experts of Toray-Research Center, the result in Fig. 9(a) is interpreted as that the top 0.7 nm region was oxidized with an oxygen-to-silicon atomic concentration ratio O/Si of 1.57 by the present heat treatment, as indicated by the dashed line in Fig. 9(a). On the other hand, similar in-depth profiles of the Si, O, and H atomic concentrations were observed for the initial sample, as shown in Fig. 9(b). A thin native oxide layer was probably formed at the top surface with an O/Si of 1.3, which was lower than that of the sample heated in liquid water at 110 °C for 1 h. It is interesting that the two samples with similar atomic concentration profiles resulted in much different effective lifetimes with a high τ_{eff} (the present heat treatment) and a low τ_{eff} (initial), as shown in Figs. 4–7. Although

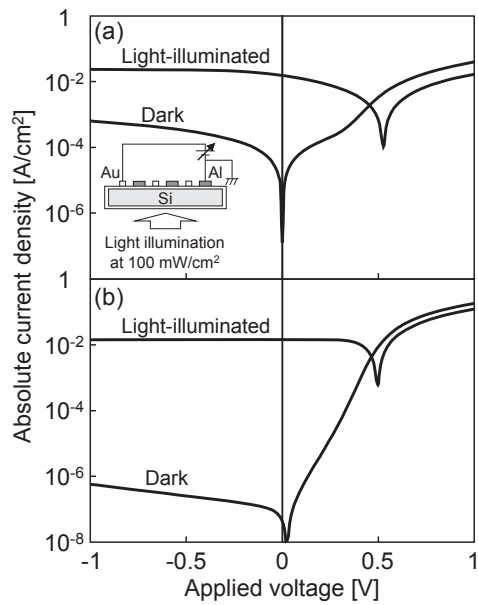


Fig. 10. The absolute electrical current density as a function of the applied voltage for MIS-type solar cell formed in sample 2 (a) and sample 3 (b) in the dark field and under AM 1.5 light illumination at 100 mW/cm² to the rear surface.

further investigation is required to clarify the physics of the present heat treatment, we propose a possibility that the present heat treatment in liquid water at 110 °C for 1 h formed continuous Si–O bonding network surface regions which successfully terminated silicon dangling bonds over a large surface area. Oxidation probably occurred uniformly via H₂O molecules in good contact with the silicon surfaces in the liquid phase. However, the results of the τ_{eff} spatial distribution shown in Figs. 4 and 5 indicate that the properties of oxide layer are not completely uniform at present. There is probably a slight spatial distribution in the thickness of the oxide layer.

Figure 10 shows the absolute electrical current density as a function of the applied voltage for the MIS-type solar cell formed in sample 2 (a) and sample 3 (b) in the dark field and under AM 1.5 light illumination at 100 mW/cm² to the rear surface. Bias voltage was applied to the Au electrode, and the Al electrode was kept at 0 V, as shown in the inset in Fig. 10. The absolute electrical current density in the dark field showed good rectified characteristics for samples 2 and 3. The rectified characteristics experimentally demonstrate that the difference in work function between the Al and Au electrodes caused the built-in potential in the silicon surface regions. Because the initial Fermi level of 4.4 eV for the n-type silicon is near the work function of Al of 4.18 eV but much different from that of Au of 5.1 eV,⁴²⁾ a large internal potential distribution associated with the depletion region is spatially formed near the Au metal electrode. On the other hand, because the initial Fermi level of 4.9 eV for the p-type silicon is near the work function of Au but much different from that of Al, a large internal potential distribution associated with the depletion region is spatially formed near the Al metal electrode. The absolute current density in the dark field was small at the reverse bias, especially, for sample 3. This indicates that the depletion layer with a low density of carrier recombination defects was formed under

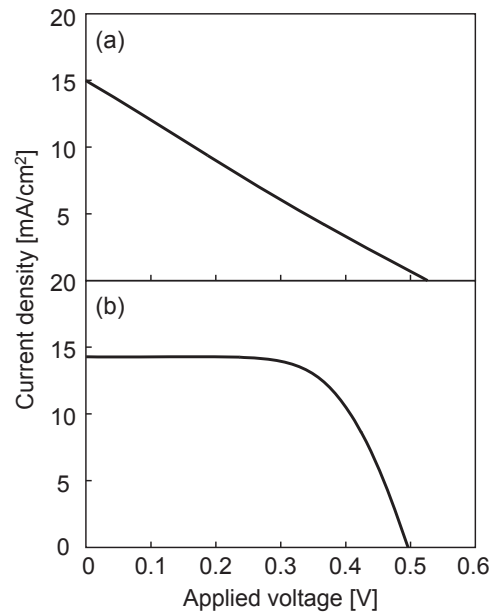


Fig. 11. Solar cell characteristics for sample 2 (a) and sample 3 (b).

the Au or Al electrode. Increasing the absolute current density in the dark field at small forward bias indicates that the silicon surface had a low density of defect states and that the passivation oxide film was sufficiently thin to flow the tunneling current. Light illumination markedly increased the absolute electrical current density. The substantially absolute electrical current density at 0 V, indicating the short circuit current density J_{sc} , indicates that photo-induced holes and electrons carriers generated in the rear surface region separated from each other and flowed into the Au and Al electrodes, respectively, in accordance with the internal built-in potential. The voltage with no absolute electrical current density, indicating the open circuit voltage V_{oc} , appeared at 0.52 and 0.49 V for samples 2 and 3, respectively. This means that electrical power was generated by AM 1.5 light illumination to the samples.

Figure 11 shows the solar cell characteristics of sample 2 (a) and sample 3 (b) obtained from the light-illuminated current voltage characteristics in Fig. 10. In the case of sample 2, J_{sc} , V_{oc} , and the fill factor (FF) were 15.3 mA/cm², 0.52 V, and 0.24, respectively. V_{oc} of 0.52 V indicates that the silicon surface passivation layer successfully formed by the present heat treatment allowed for the generation of the built-in potential underlying the Au electrode. However, the FF was very low. It results from a high series resistivity of 39 Ωcm^2 , which limited the electrical current density. The reduction in the high series resistivity is a technical problem to be overcome by processing technology improvements, for example, the optimization of the configuration of metal electrodes. In the case of sample 3, J_{sc} , V_{oc} , and FF were 14.3 mA/cm², 0.49 V, and 0.65, respectively. The series resistivity was rather low at 8 Ωcm^2 . Although there was no anti-reflection layer on the rear surface for increasing incident light intensity, the results in Figs. 10 and 11 fundamentally demonstrate a capability of application of the present passivation method to solar cell fabrication.

In this paper, we reported the passivation of silicon surfaces by heat treatment in liquid water at 110 °C, which gives

a capability of passivation processing at low temperatures, low cost, and simple steps. The thin-film passivation oxide layer allows for the flow of tunneling current. This gives a possibility of application of the present technique to the passivation of current-flowing surfaces such as surfaces of pn junction. Further investigations are necessary to demonstrate the use of different kinds of substrates especially substrates with high doping concentrations, and to establish stable passivation characteristics over the whole substrate area.

4. Conclusions

We demonstrated the passivation of silicon surfaces by heating single-crystalline silicon in liquid water at 110 °C for 1 h. The present heat treatment achieved a high τ_{eff} of 2.1×10^{-3} s for the n-type sample, which was comparable to that of 2.7×10^{-3} s for the n-type sample coated with thermally grown SiO₂ layers. The present heat treatment in liquid water achieved stable passivation with high τ_{eff} values in the range from 8.3×10^{-4} to 3.1×10^{-3} s and from 1.2×10^{-4} to 6.0×10^{-4} s under 635 nm light illumination for the n- and p-type samples, while the τ_{eff} values of the initial samples were lower than 1.2×10^{-5} s. S was estimated to be in the range from 7 to 34 cm/s and from 49 to 250 cm/s for the n- and p-type heat-treated samples, respectively, while they were in the range from 5000 to 10000 cm/s and from 30000 to 50000 cm/s for the initial n- and p-type samples, respectively. τ_{eff} maintained high values at 570 h after heat treatment for both samples. τ_{eff} for the 1.7 Ω cm n-type sample was increased from 1.2×10^{-5} to 9.5×10^{-5} s for the 635 nm light illumination by the present heat treatment. The photo-conductivity of the 17 Ω cm n-type sample was increased from 3.8×10^{-3} (initial) to 1.4×10^{-1} S/cm by the present heat treatment. The photo-conductivity roughly gave a high τ_{eff} of 6.2×10^{-4} s, which was comparable to that analyzed by microwave transmittance measurement. HR-RBS and HR-HFS analyses showed the formation of a thin oxide layer with a thickness of approximately 0.7 nm and an O/Si of 1.57. MIS-type solar cells were demonstrated with Al and Au metal formation on a top passivated surface. Electrical current as a function of voltage in a dark field demonstrated rectified characteristics. AM 1.5 light illumination at 100 mW/cm² to the rear surface resulted in the solar cell characteristics of J_{sc} , V_{oc} , and FF of 15.3 mA/cm², 0.52 V, and 0.24 for the n-type sample, and 14.3 mA/cm², 0.49 V, and 0.65 for the p-type sample, respectively. These results indicate that the present passivation method in water at 110 °C has a capability of application to photo-sensors and photo-voltaic devices.

Acknowledgments

This work was partly supported by Grants-in-Aid for Scientific Research C (No. 25420282) from the Ministry of Education, Culture, Sports, Science and Technology of Japan, The Naito Science and Engineering Foundation, and Sameken Co., Ltd.

1) S. M. Sze, *Semiconductor Devices* (Wiley, New York, 1985) Chap. 7.

2) E. A. G. Webster, L. A. Grant, and R. K. Henderson, *IEEE Trans. Electron Devices* **60**, 1188 (2013).

- 3) S. E. Bohndiek, C. D. Arvanitis, G. J. Royle, A. T. Clark, J. P. Crooks, M. L. Prydderch, R. Turchetta, A. Blue, V. O'Shea, and R. D. Speller, *Opt. Eng.* **46**, 124003 (2007).
- 4) E. A. G. Webster, L. A. Grant, and R. K. Henderson, *IEEE Electron Device Lett.* **33**, 1589 (2012).
- 5) C. D. Arvanitis, S. E. Bohndiek, G. J. Royle, A. Blue, H. X. Liang, A. Clark, M. Prydderch, R. Turchetta, and R. D. Speller, *Med. Phys.* **34**, 4612 (2007).
- 6) A. Rohatagi, Proc. 3rd World Conf. Photovoltaic Energy Conversion, 2003, A29.
- 7) M. A. Green, *Prog. Photovoltaics* **17**, 183 (2009).
- 8) M. A. Green, K. Emery, Y. Hishikawa, W. Warta, and E. D. Dunlop, *Prog. Photovoltaics* **20**, 12 (2012).
- 9) J. Zhao, A. Wang, M. A. Green, and F. Ferrazza, *Appl. Phys. Lett.* **73**, 1991 (1998).
- 10) G. S. Kousik, Z. G. Ling, and P. K. Ajmera, *J. Appl. Phys.* **72**, 141 (1992).
- 11) J. M. Borrego, R. J. Gutmann, N. Jensen, and O. Paz, *Solid-State Electron.* **30**, 195 (1987).
- 12) G. W. 't Hooft, C. Van Oordorp, H. Veenvliet, and A. T. Vink, *J. Cryst. Growth* **55**, 173 (1981).
- 13) H. Daio and F. Shimura, *Jpn. J. Appl. Phys.* **32**, L1792 (1993).
- 14) J. Sritharathikhun, C. Banerjee, M. Otsubo, T. Sugiura, H. Yamamoto, T. Sato, A. Limmanee, A. Yamada, and M. Konagai, *Jpn. J. Appl. Phys.* **46**, 3296 (2007).
- 15) Y. Takahashi, J. Nigo, A. Ogane, Y. Uraoka, and T. Fuyuki, *Jpn. J. Appl. Phys.* **47**, 5320 (2008).
- 16) M. Boulou and D. Bois, *J. Appl. Phys.* **48**, 4713 (1977).
- 17) Y. Ogita, *J. Appl. Phys.* **79**, 6954 (1996).
- 18) C. Munakata, *Jpn. J. Appl. Phys.* **43**, L1394 (2004).
- 19) J. W. Corbett, J. L. Lindström, S. J. Pearton, and A. J. Tavendale, *Sol. Cells* **24**, 127 (1988).
- 20) Y. Lariionova, V. Mertens, N.-P. Harder, and R. Brendel, *Appl. Phys. Lett.* **96**, 032105 (2010).
- 21) B. L. Sopori, X. Deng, J. P. Benner, A. Rohatagi, P. Sana, S. K. Estreicher, Y. K. Park, and M. A. Roberson, *Sol. Energy Mater. Sol. Cells* **41–42**, 159 (1996).
- 22) I.-W. Wu, A. G. Lewis, T.-Y. Huang, and A. Chiang, *IEEE Electron Device Lett.* **10**, 123 (1989).
- 23) J. Schmidt, M. Kerr, and A. Cuevas, *Semicond. Sci. Technol.* **16**, 164 (2001).
- 24) J. Schmidt, A. Merkle, R. Brendel, B. Hoex, M. C. M. van de Sanden, and W. M. M. Kessels, *Prog. Photovoltaics* **16**, 461 (2008).
- 25) J. Takenezawa, M. Hasumi, T. Sameshima, T. Koida, T. Kaneko, M. Karasawa, and M. Kondo, *J. Non-Cryst. Solids* **358**, 2285 (2012).
- 26) T. Sameshima and M. Satoh, *Jpn. J. Appl. Phys.* **36**, L687 (1997).
- 27) T. Sameshima, M. Satoh, K. Sakamoto, K. Ozaki, and K. Saitoh, *Jpn. J. Appl. Phys.* **37**, 4254 (1998).
- 28) K. Sakamoto and T. Sameshima, *Jpn. J. Appl. Phys.* **39**, 2492 (2000).
- 29) T. Sameshima, H. Hayasaka, M. Maki, A. Masuda, T. Matsui, and M. Kondo, *Jpn. J. Appl. Phys.* **46**, 1286 (2007).
- 30) K. Asada, K. Sakamoto, T. Watanabe, T. Sameshima, and S. Higashi, *Jpn. J. Appl. Phys.* **39**, 3883 (2000).
- 31) T. Sameshima, K. Kogure, and M. Hasumi, *Jpn. J. Appl. Phys.* **49**, 110205 (2010).
- 32) R. Har-Lavan and D. Cahen, *IEEE J. Photovoltaics* **3**, 1443 (2013).
- 33) B. Kuhlmann, A. G. Aberle, R. Hezel, and G. Heiser, *IEEE Trans. Electron Devices* **47**, 2167 (2000).
- 34) S.-H. Lo, D. A. Buchanan, Y. Taur, and W. I. Wang, *IEEE Electron Device Lett.* **18**, 209 (1997).
- 35) T. Sameshima, H. Hayasaka, and T. Haba, *Jpn. J. Appl. Phys.* **48**, 021204 (2009).
- 36) T. Sameshima, T. Nagao, S. Yoshidomi, K. Kogure, and M. Hasumi, *Jpn. J. Appl. Phys.* **50**, 03CA02 (2011).
- 37) T. Sameshima, R. Ebina, K. Betsuin, Y. Takiguchi, and M. Hasumi, *Jpn. J. Appl. Phys.* **52**, 011801 (2013).
- 38) E. D. Palk, *Handbook of Optical Constants of Solids* (Academic Press, London, 1985) p. 547.
- 39) A. S. Grove, *Physics and Technology of Semiconductor Devices* (Wiley, New York, 1967) Chap. 5.
- 40) J. W. Orton and P. Blood, *The Electrical Characterization of Semiconductors: Measurement of Minority Carrier Properties* (Academic Press, London, 1990) Chap. 4.
- 41) F. Feldmann, M. Simon, M. Bivour, C. Reichel, M. Hermle, and S. W. Glunz, *Appl. Phys. Lett.* **104**, 181105 (2014).
- 42) H. B. Michaelson, *J. Appl. Phys.* **48**, 4729 (1977).